Mechanism and Simulation of Electrochemical Current Oscillations Observed in the H_2O_2-Reduction Reaction on Platinum Electrodes in Acidic Solutions

Yoshiharu Mukouyama, Hayato Hommura, Shuji Nakanishi, Takashi Nishimura, Hidemitsu Konishi, and Yoshihiro Nakato*

Department of Chemistry, Graduate School of Engineering Science, and Research Center for Photoenergetics of Organic Materials, Osaka University, Toyonaka, Osaka 560-8531

(Received January 5, 1999)

Mechanisms of electrochemical current oscillations of two types, named oscillation A and B, both observed for the H_2O_2-reduction reaction on Pt electrodes in acidic solutions, have been studied experimentally and by mathematical simulation. Oscillation A appears in a potential region just before hydrogen evolution, while oscillation B appears in a region of hydrogen evolution. A phase diagram we obtained has shown that oscillations A and B appear in limited ranges of the H^+ and H_2O_2 concentrations and their ratio. The oscillation period for oscillation A increases with decreasing H_2O_2 concentration and negative shift of the electrode potential, mainly determined by the current density in the low-current state. Mathematical simulation by taking account of all plausible interfacial reactions (H_2O_2 reduction, hydrogen adsorption, and hydrogen evolution) reproduces the essential features of oscillation A, but does not reproduce oscillation B. It is shown that a positive feedback mechanism works in sudden transitions between the high- and low-current states for oscillation A.

Electrochemical oscillations have been reported for various systems as summarized in recent reviews,[1—3] including anodic metal dissolution,[4,5] cathodic metal deposition,[6] oxidation of hydrogen,[7] and small organic compounds,[8,9] and reduction of hyrogen peroxide,[10—16] peroxodisulfate,[17] etc. The oscillation phenomena are interesting from the point of view of dynamic self-organization of molecular systems. Moreover, understanding of the mechanism will give new insights into development of new types of devices as well as understanding of various biological functions.

For deep understanding of the mechanisms of electrochemical oscillations, it is very important to clarify reaction schemes and reproduce the oscillations by mathematical simulation. Such work, however, seems to be still rather limited. The first mathematical model for electrochemical oscillations was proposed by Franck and FitzHugh[4] to explain current oscillations in anodic dissolution reactions of iron electrodes in acid solutions. Recently, an interesting and simpler mathematical model was developed by Koper and Sluyters[18,19] for modelling oscillations involving metal deposition[18] and metal dissolution,[19] and later applied to oscillating H_2O_2-reduction reactions on p-$CuInSe_2$[20] and n-GaAs.[21] Unfortunately, the oscillating reactions for reported systems[4,18—21] in most cases include dissolution of electrodes themselves and seem to be too complicated to be fully understood by mathematical models.

We reported in previous papers[22—25] that a new type of electrochemical oscillation, called oscillation B, was observed, in addition to a reported one,[14,15] called oscillation A in our papers,[22—25] in the H_2O_2-reduction reaction on Pt electrodes in aqueous H_2SO_4. These oscillations are interesting for the following reasons: (1) The Pt electrode is stable during oscillations, only acting as an electrocatalyst. (2) Hydrogen evolution, hydrogen adsorption, and H_2O_2 reduction, by which the oscillations are caused as explained later, are the simplest electrochemical reactions. This makes the mechanistic study easier. (3) Oscillation A is observed in a potential region just before hydrogen evolution, while oscillation B is observed in a potential region of hydrogen evolution. That is, two types of oscillations are observed in one "H_2O_2–H_2SO_4–Pt" system, depending on the electrode potential. This should also facilitate the mechanistic study.

In a previous paper[23] we reported the general features and fundamental reaction models for oscillations A and B. In this paper we report more detailed experimental results and results of mathematical simulation, which have not only confirmed the previously proposed reaction model but also revealed the essential mechanism of the oscillation.

Experimental

Electrochemical measurements were done using a normal three-electrodes system. The working electrode was a circular Pt disc of 0.785 mm^2 in area, held in a glass tube. The Pt disc was prepared by firing a fine Pt wire (99.97% in purity), followed by polishing of a resultant Pt sphere with alumina powder. The front (electrochemically active) surface of the Pt disc was kept vertical in an electrochemical cell and placed in a static manner without any rotating mechanism. No solution stirring nor nitrogen-gas bub-

bling was done. For such a static working electrode, simpler and better-defined oscillations were observed, as reported in a previous paper.[23] The counter electrode was a Pt plate (10×10 mm^2 in area), and the reference electrode was a saturated calomel electrode (SCE). The tip of the SCE was put just below the Pt disc electrode so that it might cause little disturbance in the current flow around the working electrode. Ohmic drops were not corrected unless otherwise noted.

The Pt-disc electrodes were washed in acetone and concentrated nitric acid and immersed in 0.5 M H_2SO_4 and 0.7 M H_2O_2 (M = mol dm^{-3}) before use. Aqueous electrolyte solutions were prepared using special grade chemicals and water purified from deionized water with a Milli-Q water purification system. All electrochemical measurements were done using freshly prepared electrolyte solutions.

Current density (j) vs. potential (U) curves and current (or potential) vs. time (t) curves were measured with a Hokuto-Denko HA-501 potentiogalvanostat and a Nikko-Keisoku NPS-2 potential programmer. They were either recorded with a National VP-6415A X–Y recorder or stored digitally at 1 kHz with a Mac ADIOS II/16 (GW Instruments).

Results

Figure 1 shows current density (j) vs. potential (U) curves for a Pt disc electrode in 0.10 M H_2SO_4 containing H_2O_2 in various concentrations, measured under a potential-controlled condition. The j–U curve in Fig. 1(a) is for 0.10 M H_2SO_4 with no H_2O_2, which is included to indicate cathodic and anodic current peaks (in a region from +0.09 to −0.28 V vs. SCE) due to formation and disappearance of adsorbed hydrogen atoms, called upd-H (under-potential deposited hydrogen), which are important in the appearance of the oscillations, as discussed later. (Note that the current–density scale in Fig. 1(a) is quite different from that in Fig. 1(b)—(d).) For an H_2O_2 concentration of 0.1 M (Fig. 1(b)), a cathodic current due to H_2O_2 reduction starts at about 0.6 V vs. SCE and reaches the diffusion-limited current at around 0.40 V. The j–U curve shows the "negative slope" in a region from −0.28 to −0.33 V, and then a hydrogen evolution current starts in a more negative potential. No oscillation is observed for this H_2O_2 concentration. For a slightly higher H_2O_2 concentration of 0.3 M (Fig. 1(c)), both oscillations A and B appear in potential regions of the "negative slope" and hydrogen evolution, respectively. For a much higher H_2O_2 concentration of 0.7 M (Fig. 1(d)), both oscillations A and B disappear. A similar H_2O_2-concentration dependence was reported in a previous paper[23] for another H_2SO_4 concentration.

These results clearly indicate that oscillations A and B appear in limited ranges of the H_2O_2 and H_2SO_4 concentrations. To make the ranges clearer and obtain a phase diagram with respect to the H_2O_2 and H_2SO_4 concentrations, we did experiments for various sets of the H_2O_2 and H_2SO_4 concentrations. The results are summarized in Fig. 2. We can see that not only the H_2O_2 and H_2SO_4 concentrations but also their ratio are important for the appearance of oscillations A and B.

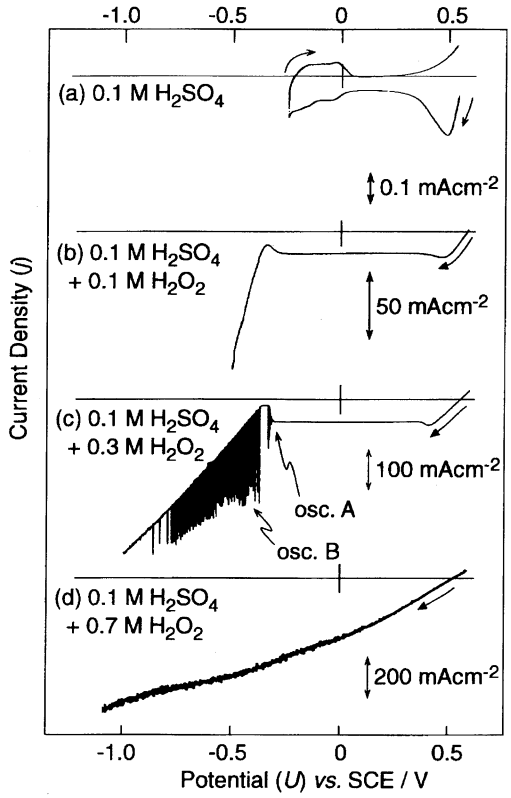

Fig. 1. Current density (j)–potential (U) curves for a polycrystalline Pt disc electrode in 0.10 M H_2SO_4 with H_2O_2 in various concentrations, measured under a potential-controlled condition. The scan rate is 10 mV s^{-1}.

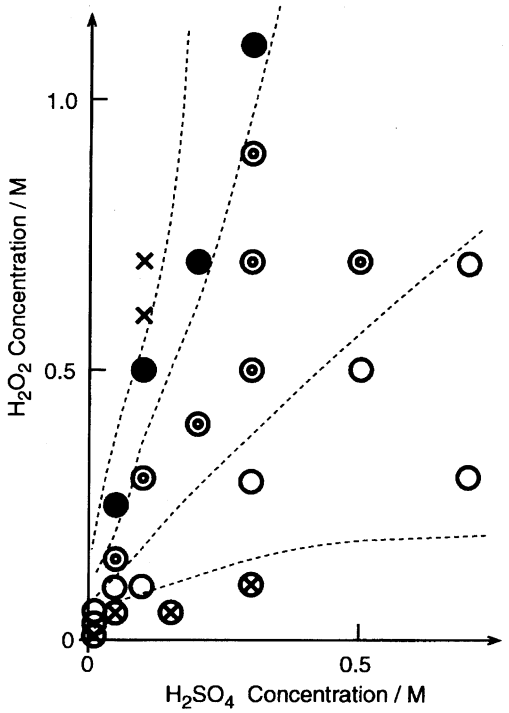

Fig. 2. A phase diagram with respect to the H_2O_2 and H_2SO_4 concentrations. ⊗: no oscillation, though the negative resistance appears (cf. Fig. 1(b)), ○: only oscillation A appears, ◎: both oscillations A and B appear, ●: only oscillation B appears, and ×: no oscillation nor negative resistance appears (cf. Fig. 1(c)).

Figure 3 shows the influence of the H_2O_2 concentration on the oscillation pattern (waveform) for oscillation A. Figure 4 summarizes the results of similar experiments, by plotting the current densities (j_1—j_4) and oscillation periods (T, t_1 and t_2), which characterize the waveform (see the upper diagram in Fig. 4), as a function of the H_2O_2 concentration. The duration of the high-current state (t_1) increases gradually with increasing H_2O_2 concentration, but the duration of the low-current state (t_2) decreases largely, and thus the oscillation period (T) decreases with increasing H_2O_2 concentration. On the other hand, the current densities, j_2, j_3, and j_4, are all nearly constant, irrespective of the H_2O_2 concentration, except that the j_1 increases slightly with the H_2O_2 concentration. The nearly constant j_2 and j_3 strongly suggest that these j_2 and j_3 decide the durations t_1 and t_2; namely, when the current density in the high-current state reaches a critical value j_2, then it drops sharply, and when the current density in the low-current state reaches another critical value j_3, it rises sharply.

Figure 5 shows the influence of the electrode potential on the oscillation pattern for oscillation A in 0.7 M H_2O_2 + 0.3 M H_2SO_4. The durations of the high- and low-current states (t_1 and t_2) and the oscillation period (T) as well as the peak current density (j_1) all increase with negative shift of the electrode potential (U). In particular, at a large negative potential of −320 mV vs. SCE, the duration of the low-current state (t_2) becomes much longer, which finally turns into the disappearance of oscillation A (infinitely long t_2) at a more negative potential.

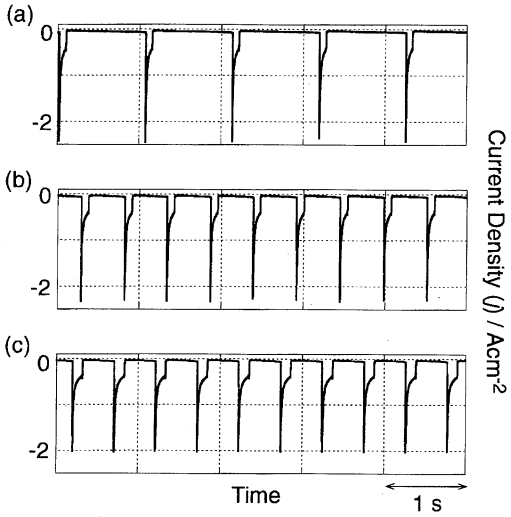

Fig. 3. Effect of the H_2O_2 concentration on the oscillation pattern (waveform) for oscillation A at −0.32 V vs. SCE. The H_2O_2 concentration is (a) 0.6 M, (b) 0.7 M, and (c) 0.8 M. The H_2SO_4 concentration is 0.3 M in all cases.

Simulation

1. Reaction Model. In a previous paper[23] we proposed fundamental reaction models for oscillations A and B: The high- and low-current states for oscillation A correspond to active H_2O_2 reduction in the absence of upd-H and strong suppression of the H_2O_2 reduction by formation of upd-H of

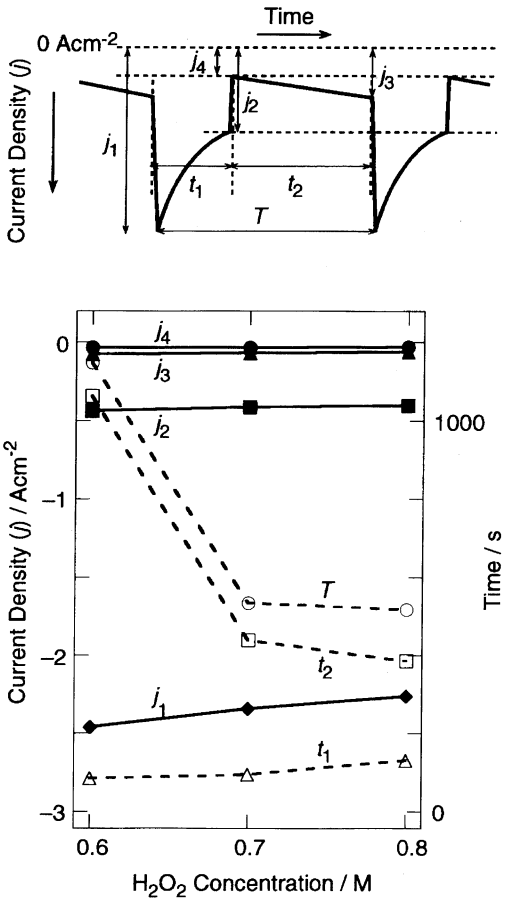

Fig. 4. Dependence of the current density and oscillation period on the H_2O_2 concentration for oscillation A at −0.30 V vs. SCE. The H_2SO_4 concentration is 0.3 M in all cases.

a nearly full coverage, respectively, and those for oscillation B correspond to active H_2O_2 reduction and hydrogen evolution, respectively. Thus we have attempted mathematical simulation to investigate the models in more detail. From the models and also from the j–U curves in Fig. 1, we can expect that oscillations A and B are caused by H_2O_2 reduction, formation of upd-H, and hydrogen evolution. Thus the following reactions have been taken into account in the present simulation:

$$Pt + H_2O_2 + H^+ + e^- \xrightarrow{k_1} Pt\text{-}OH + H_2O \quad (1a)$$

$$Pt\text{-}OH + H^+ + e^- \xrightarrow{k_1'} Pt + H_2O \quad (1b)$$

$$Pt + H^+ + e^- \underset{k_{-2}}{\overset{k_2}{\rightleftharpoons}} Pt\text{-}H\ (upd\text{-}H) \quad (2)$$

$$Pt + H^+ + e^- \underset{k_{-3}}{\overset{k_3}{\rightleftharpoons}} Pt\text{-}H\ (on\text{-}top\ H) \quad (3)$$

$$Pt\text{-}H\ (on\text{-}top\ H) + Pt\text{-}H\ (on\text{-}top\ H) \xrightarrow{k_4} H_2 \quad (4)$$

$$H_2 \xrightarrow{k_5} 2H^+ + 2e^- \quad (5)$$

where Pt represents schematically the surface site(s) at the Pt electrode.

It is reported in the literature[26,27] that the H_2O_2 reduction on Pt electrodes proceeds by a two-step mechanism. We ten-

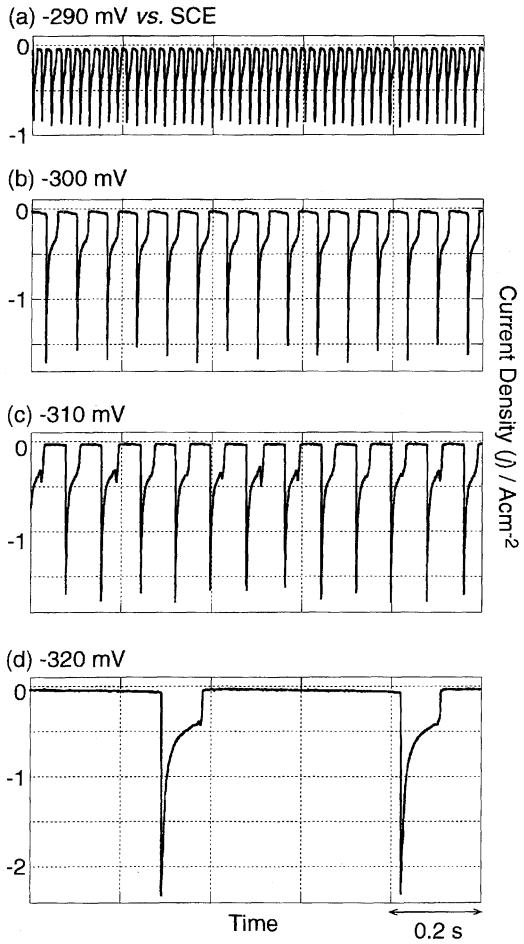

Fig. 5. Effect of the electrode potential (U) on the oscillation pattern for oscillation A in 0.7 M H_2O_2 + 0.3 M H_2SO_4.

tatively assume in this work that the H_2O_2 reduction on Pt proceeds via adsorbed reaction intermediate(s) as indicated in Eqs. 1a and 1b. The assumption of (dissociative) H_2O_2 adsorption seems to be important to explain the aforementioned suppression of the H_2O_2 reduction by the formation of upd-H. We also tentatively assume, for simplicity, that reaction (1a), which is expected to occur only on a part of the naked Pt surface not covered with upd-H, is a rate-determining step,[28] in order to take into account the effect of upd-H in the rate equations discussed later.

Reaction (2) represents the formation and disappearance of upd-H. These processes are observed as two cathodic and anodic current peaks at around -0.06 and -0.19 V vs. SCE (see Fig. 1(a)) for polycrystalline Pt electrodes,[29,30] as already mentioned in the preceding section. The upd-H is stable, located at three- or four-fold symmetry sites of surface Pt lattices, and does not contribute to hydrogen evolution.[30,31] It is to be noted that the "negative slope" in Fig. 1(b) appears in potentials more negative than the second cathodic current peak at -0.19 V in Fig. 1(a), i.e., in potentials where the Pt surface is almost fully covered with upd-H. This implies that the H_2O_2 reduction is suppressed only by the formation of upd-H of a nearly full coverage.

Reactions (3) and (4) represent hydrogen evolution, which is observed as a monotonously increasing cathodic current starting at about -0.33 V vs. SCE (Figs. 1(a) and 1(b)). It is known[29] that hydrogen evolution on Pt electrodes proceeds by the Volmer–Tafel mechanism, i.e., via formation of adsorbed hydrogen atoms followed by their mutual combination just as shown in reactions (3) and (4). Recent experiments have shown[30,31] that adsorbed H atoms contributing to hydrogen evolution are not upd-H, as mentioned above, but ones of another type, called "on-top H", which may be formed on a Pt surface covered with upd-H. Reaction (5) represents oxidation of hydrogen, the reaction mechanism of which is not yet fully clarified. Kita et al. suggested[31] that the rate-determining steps might be different between hydrogen oxidation and evolution. Reaction (5) is tentatively included to take into account the influence of the surface H_2 concentration without assuming any reaction intermediate at the Pt surface.

2. Mathematical Equations. Mathematical equations for simulating oscillations A and B have been constructed as follows. First, the rate constants for reactions (1)—(3) and (5) are assumed to be expressed by the following Butler–Volmer equations,

$$k_i(E) = k_{i0} \exp[-\alpha n F(E - E_{i0})/RT] \quad \text{for } i = 1,\ 2,\ \text{and } 3 \tag{6}$$

$$k_i(E) = k_{i0} \exp[(1 - \alpha) n F(E - E_{i0})/RT] \quad \text{for } i = -2,\ -3,\ \text{and } 5 \tag{7}$$

where E is the (true) electrode potential (cf. Fig. 7), k_i the rate constant for the i-th reaction ($i = 1$, ± 2, ± 3, and 5), k_{i0} the rate constant at $E = E_{i0}$, E_{i0} the equilibrium redox potential for the i-th reaction, α the transfer coefficient, n the number of transferred electrons, F the Faraday constant, R the gas constant, and T the temperature. In this work, $\alpha = 1/2$ is assumed for all reactions for simplicity. Because reactions 2 and -2 (and 3 and -3) are reverse reactions to each other, we obtain $E_{20} = E_{-20}$ and $E_{30} = E_{-30}$.

The time dependence of the concentration of H_2O_2 at the electrode surface, C^s_{HO}, is expressed according to a Koper–Sluyters model[18,19] as follows:

$$(\delta_{HO}/2)\mathrm{d}C^s_{HO}/\mathrm{d}t = (D_{HO}/\delta_{HO})(C^b_{HO} - C^s_{HO}) - k_1 C^s_{HO} C^s_{H^+}(1 - \theta_H), \tag{8}$$

where D_{HO} is the diffusion coefficient for H_2O_2, δ_{HO} the thickness of the diffusion layer for H_2O_2, C^b_{HO} the concentration of H_2O_2 in the solution bulk, $C^s_{H^+}$ the concentration of H^+ ions at the electrode surface, and θ_H the surface coverage of upd-H. The first term on the right-hand side represents the increase in C^s_{HO} by diffusion, while the second term does the decrease in C^s_{HO} by the electrochemical reaction (1a). The introduction of $(1 - \theta_H)$ in the second term expresses that reaction (1a) proceeds only on the part of the naked Pt surface not covered with upd-H, as mentioned before. The amount of the naked Pt surface is taken to be proportional to $(1 - \theta_H)$ because the surface coverages for H_2O_2-related adsorbed species such as Pt-OH are negligibly small under

the aforementioned assumption that reaction (1a) is a rate-determining step. In the first term of the right-hand side of Eq. 8, we adopt a model of Nernst's diffusion layer having a constant thickness (δ_{HO}), as is generally done by other workers.[4,18—21] This is mainly due to a limitation of calculation capacity in our calculation program. The term ($\delta_{HO}/2$) on the left-hand side of Eq. 8 is added to take an average of the H_2O_2 concentration in the diffusion layer as explained in detail by Koper and Sluyters.[18,19]

The time dependence of the concentration of H^+ ions at the electrode surface, $C^s_{H^+}$, is expressed, similarly to C^s_{HO}, with a small contribution of the drift motion of H^+ being neglected as in the literature,[18,19] as follows:

$$(\delta_{H^+}/2)\mathrm{d}C^s_{H^+}/\mathrm{d}t = (D_{H^+}/\delta_{H^+})(C^b_{H^+} - C^s_{H^+}) + \{-2k_1 C^s_{HO} C^s_{H^+}(1-\theta_H) - k_2 C^s_{H^+}(1-\theta_H) + k_{-2}\theta_H - k_3 C^s_{H^+}(1-\Theta_H) + k_{-3}\Theta_H + 2k_5 p_{H_2} \quad (9)$$

where D_{H^+} is the diffusion coefficient for H^+ ions, δ_{H^+} the thickness of the diffusion layer for H^+, $C^b_{H^+}$ the concentration of H^+ in the solution bulk, Θ_H the surface coverage of the "on-top H", and p_{H_2} the pressure of H_2 at the electrode surface. The p_{H_2} is taken to be proportional to the rate of hydrogen evolution ($p_{H_2} = ak_4\Theta_H^2$, a = constant) owing to a limitation of the calculation program.

The surface coverage of upd-H, θ_H, can be expressed as a function of the (true) electrode potential, E, and $C^s_{H^+}$, by taking into account that the forward and backward processes of reaction (2) are in equilibrium at every electrode potential E. Under the aforementioned assumption that the surface coverages of H_2O_2-related adsorbed species are negligibly small, the equilibrium condition is given as follows:

$$k_2 C^s_{H^+}(1-\theta_H) = k_{-2}\theta_H. \quad (10)$$

By using Eqs. 6 and 7 for k_2 and k_{-2} together with $\alpha = 1/2$, $n = 1$, and $E_{20} = E_{-20}$ mentioned before and also by taking account of an approximate relation

$$C^s_{H^+}\ (\text{in a unit of mol cm}^{-3}) = 10^{-3}\exp\{\ln C^s_{H^+}\ (\text{in a unit of mol dm}^{-3})\} \cong 10^{-3}\exp\{-(\ln 10)p\mathrm{H}^s\}$$

we obtain the following expression for θ_H

$$\theta_H \cong 1/[1+(k_{-20}/k_{20}10^{-3})\exp\{(F/RT)(E-E_{20}+\beta p\mathrm{H}^s)\}] \quad (11)$$

where $\beta = RT(\ln_e 10)/F \cong 0.059$ V at 300 K and $p\mathrm{H}^s$ the solution $p\mathrm{H}^s$ near the electrode surface. In this work, however, we use another expression, Eq. 12, instead of Eq. 11,

$$\theta_H = 1/[1+(k_{-20}/k_{20}10^{-3})\exp\{b(E-E_{20}+\beta p\mathrm{H}^s)\}] \quad (12)$$

with b being taken as a parameter. This is because, in Eq. 11, the presence of only one kind of upd-H is considered, though the observed j–U curve shows two current peaks for upd-H (Fig. 1(a)), i.e., the presence of (at least) two kinds of upd-H. The parameter b is determined such that θ_H changes over a potential region of the observed two current peaks. Figure 6 shows a θ_H vs. E relation calculated with $b = 80\ \mathrm{V}^{-1}$ and

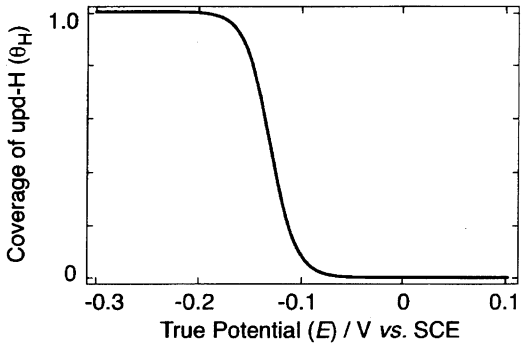

Fig. 6. The surface coverage of upd-H (θ_H) as a function of E, calculated by Eq. 12 with $b = 80\ \mathrm{V}^{-1}$, $(k_{-20}/k_{20}\times 10^{-3}) = 1$, $E_{20} = -0.10$ V vs. SCE, and $p\mathrm{H}^s = 0.53$.

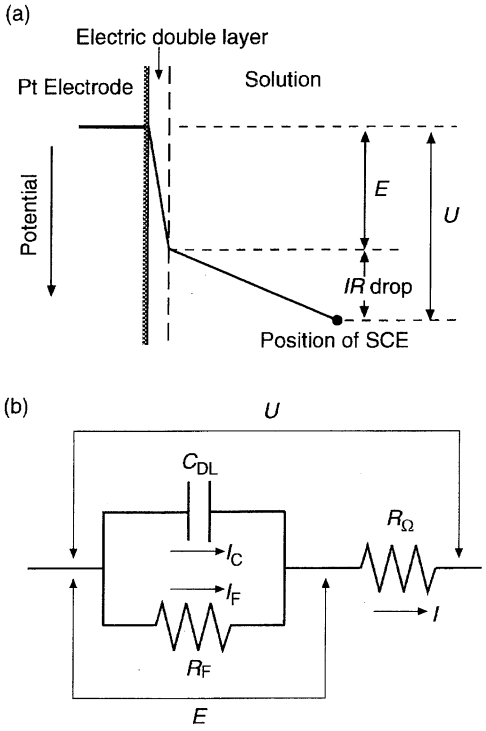

Fig. 7. (a) Schematic potential profile for the region between the electrode surface and the position of SCE, and (b) an equivalent circuit for the electrode including the above region.

$p\mathrm{H}^s = 0.52$. We can see that θ_H changes from nearly zero to one in a potential (E) range of about -0.07 to -0.2 V vs. SCE.

Now let us consider the j–U curve, i.e., the relation between the current density (j) and the (external or applied) electrode potential (U). From an equivalent circuit for the Pt electrode (Fig. 7(b)) together with an expected potential profile (Fig. 7(a)), the following equation is derived according to Koper and Sluyters,[18,19]

$$I = jA = (U-E)/R_\Omega = I_C + I_F = AC_{DL}(\mathrm{d}E/\mathrm{d}t) + I_F \quad (13)$$

where I is the total current, A the electrode area, $(U-E)$ is the ohmic drop between the electrode surface and the position of SCE, R_Ω the solution resistance between the electrode

surface and the position of SCE, $I_C = AC_{DL}$ (dE/dt) is the charging current, C_{DL} the double-layer capacitance, and I_F the Faradaic current. Equation 13 can be rewritten as

$$dE/dt = (U - E)/AC_{DL}R_\Omega - I_F/AC_{DL}. \quad (14)$$

The I_F is derived from reactions (1)—(3) and (5), under the aforementioned assumption that the surface coverages of H_2O_2-related adsorbed species are negligibly small, as follows.

$$I_F = AF\{-2k_1 C_{HO}{}^s C_{H^+}{}^s(1-\theta_H) - k_2 C_{H^+}{}^s(1-\theta_H) + k_{-2}\theta_H - k_3 C_{H^+}{}^s(1-\Theta_H) + k_{-3}\Theta_H + 2k_5 p_{H_2}\}. \quad (15)$$

Finally, the time dependence of Θ_H is expressed from reactions (3) and (4) in the following:

$$N_0 d\Theta_H/dt = k_3 C_{H^+}{}^s(1-\Theta_H) - k_{-3}\Theta_H - 2k_4\Theta_H{}^2, \quad (16)$$

where N_0 is the total amount of surface sites for "on-top H" per unit area. The Θ_H can change from 0 to 1, independent of θ_H, because the "on-top H" can be formed on a Pt surface covered with upd-H as mentioned before.

3. Calculations. We made numerical calculations using Eqs. 6, 7, 8, 9, 12, 14, 15, and 16, with j, E, C^s_{HO}, $C^s_{H^+}$, θ_H, and Θ_H being taken as time-dependent variables and other quantities such as E_{i0}, k_{i0}, b, δ_{HO}, D_{HO}, δ_{H^+}, D_{H^+}, C_{DL}, etc. taken as parameters. The (external or applied) electrode potential U is either kept constant or changed with time at a constant rate. Figures 8 and 9 show some examples of calculated results. The parameter values used for calculation are shown in the caption of Fig. 8: Some of them were taken from the literature but the others were chosen such that calculated j–U and j–t curves agreed with the observed ones. The E_{10} value was tentatively estimated from a reported value for p-GaP electrodes.[28] The $E_{20} = E_{-20}$ was estimated from the j–U curve as the center of the two current peaks for upd-H (Fig. 1(a), see also Fig. 6). The $E_{30} = E_{-30}$ was estimated from the observed hydrogen-evolution current. There are no reported data for the k_{i0} values and therefore they were roughly estimated from the rate constants reported for various metal deposition reactions ($M^{z+} + ze^- \rightarrow M$) which ranged from 10^{-1} to 10^{-4} cm s^{-1}.[32] The diffusion coefficients for H_2O_2 (D_{HO})[33—35] and H^+ (D_{H^+})[36] were taken from reported values. A difference between δ_{HO} and δ_{H^+} in the caption of Fig. 8 mainly comes from the difference between D_{HO} and D_{H^+}.

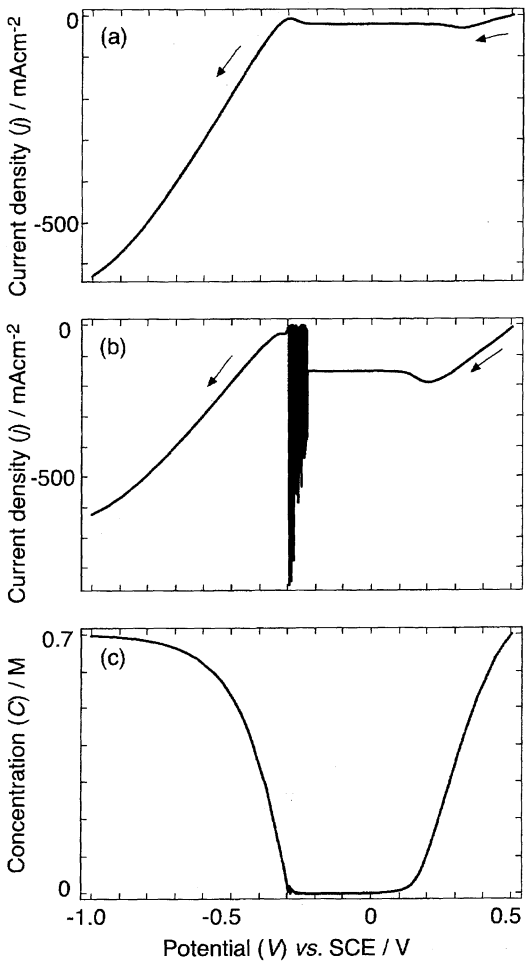

Fig. 8. Calculated j vs. U and C^s_{HO} vs. U curves with U being scanned at a rate of 0.02 V s^{-1}. Parameter values used are as follows: $C^b_{HO} = 0.7\times10^{-3}$ mol cm^{-3}, $\delta_{HO} = 0.015$ cm, $D_{HO} = 1.7\times10^{-5}$ cm^2 s^{-1}, $C^b_{H^+} = 0.3\times10^{-3}$ mol cm^{-3}, $\delta_{H^+} = 0.004$ cm, $D_{H^+} = 9.3\times10^{-5}$ cm^2 s^{-1}, $A = 0.01$ cm^2, $C_{DL} = 2.0\times10^{-5}$ F cm^{-2}, $R_\Omega = 50\Omega$, $b = 80$ V^{-1}, $k_{10} = 0.30$ mol^{-1} cm^4 s^{-1}, $k_{20} = 1.0\times10^{-5}$ cm s^{-1}, $k_{-20} = 1.0\times10^{-8}$ mol cm^{-2} s^{-1}, $k_{30} = 5.0\times10^{-3}$ cm s^{-1}, $k_{-30} = 5.0\times10^{-6}$ mol cm^{-2} s^{-1}, $k_{40} = 5.0\times10^{-6}$ mol cm^{-2} s^{-1}, k_{50} $a = 0.4$ (with p_{H_2} expressed as $p_{H_2} = ak_4\Theta_H^2$ in Eqs. 9 and 15 as mentioned before), $N_0 = 2.2\times10^{-9}$ mol cm^{-2}, $T = 300$ K, $\alpha = 0.50$, $pH^s = -\log(10^3\times C^s_{H^+})$, $E_{10} = 0.55$ V vs. SCE, $E_{20} = E_{-20} = -0.10$ V vs. SCE, and $E_{30} = E_{-30} = -0.29 - 0.059\times pH^s$ V vs. SCE.

The calculated j–U curves in Fig. 8 reproduce the essential features of the observed j–U curves shown in Figs. 1(b) and 1(c), i.e., the appearance of a negative slope in a low H_2O_2 concentration (Fig. 8(a)) and that of oscillation A in a higher H_2O_2 concentration (Fig. 8(b)). However, oscillation B does not appear in calculated j–U curves, suggesting that it is necessary to consider another factor to explain oscillation B. Further studies on this point are now in progress.

Figure 9 shows a calculated j–t curve, together with E–t, C^s_{HO}–t, $C^s_{H^+}$–t, and θ_H–t curves, at $U = -0.28$ V for oscillation A. Again, the essential features of the observed j–t curves (Figs. 3 and 5) are reproduced. In addition, this calculation reproduced the other features of the observed oscillations that the oscillation period (T) increased with decreasing H_2O_2 concentration and with decreasing electrode potential (see Figs. 3(a)—3(c) and Figs. 5(a)—5(d) in mutual comparison).

The calculated oscillation in Fig. 9(a) consists of relatively sharp current pulses, contrary to the observed oscillations, which have a longer duration time in the high-current state. This discrepancy may be due to the approximation of a Nernst diffusion layer with a constant thickness adopted in this work. As can be seen from Fig. 9(d), the deviation of the surface H^+ concentration ($C^s_{H^+}$) from the bulk one is only small because of a high mobility of H^+, contrary to the case of the surface

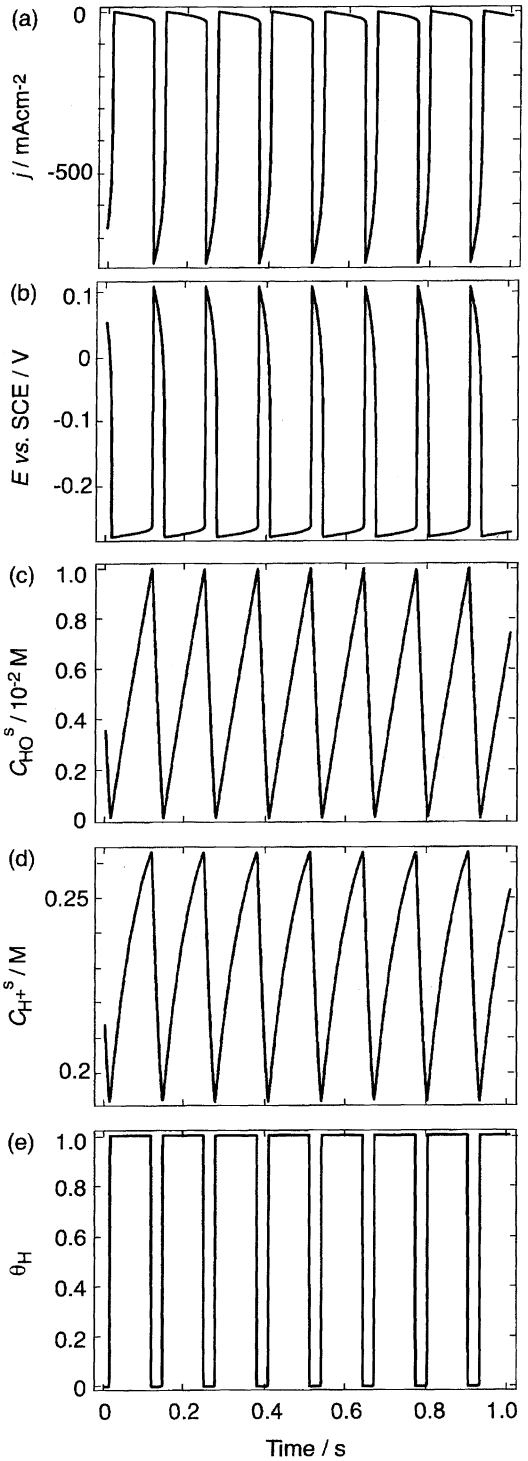

Fig. 9. Calculated j–t, E–t, C^{s}_{HO}–t, $C^{s}_{H^+}$–t, and θ_H–t curves at $U = -0.28$ V vs. SCE (which is in a potential region of oscillation A). The parameter values used are the same as in Fig. 8.

H_2O_2 concentration (C^{s}_{HO}) in Fig. 9(c). In fact, essentially the same results as Figs. 8 and 9 can be obtained by calculation under an assumption of constant $C^{s}_{H^+}$.

Discussion

As mentioned in the preceding section, this simulation has reproduced the essential features of the observed oscillation (oscillation A) well, indicating the validity of the reaction model. Also, the calculated j–t and θ_H–t curves in Fig. 9 show clearly that the high- and low-current states for oscillation A correspond to active H_2O_2 reduction in the absence of upd-H and strong suppression of the H_2O_2 reduction with a nearly full coverage of upd-H, respectively, in agreement with our previously proposed reaction model.[23]

Now let us consider by what mechanism the oscillation (the sudden increase and decrease of the current density) occurs, on the basis of the calculated results. First, let us start from the low-current state of oscillation A with very low j and $\theta_H \cong 1$. In this state, the H_2O_2 reduction hardly occurs and thus the C^{s}_{HO} increases with time by diffusion of H_2O_2 from the solution bulk (see the C^{s}_{HO}–t curve in Fig. 9(c)). Nearly in proportion to the increase in C^{s}_{HO}, the H_2O_2-reduction current (j) in the low-current state increases gradually with time (the j–t curve in Fig. 9(a)). It is to be noted here that the H_2O_2-reduction current (j) in the low-current state flows through a small amount of naked Pt sites not covered with upd-H, which is in proportion to $(1-\theta_H)$. It is to be noted also that the increase in j causes an increase in the ohmic drop in the solution and hence causes a positive shift in the true electrode potential (E) under a constant applied potential (U) (see Fig. 7(a)). Thus, the increase in j causes a positive shift in E, and the positive shift in E leads to a decrease in θ_H or an increase in $(1-\theta_H)$ (Fig. 6), which, in turn, causes a further increase in j. Here is a positive feedback mechanism for the increase in j. Thus, when the j reaches a certain critical value and the θ_H enters into the region of rapid change with E (Fig. 6), the j suddenly increases, accompanied by a sharp decrease of θ_H from nearly one to zero (the j–t and θ_H–t curves in Fig. 9).

The inverse process, i.e., a sudden change from the high-current to the low-current states (or a change from $\theta_H \cong 0$ to $\theta_H \cong 1$) can be explained similarly. If active H_2O_2-reduction reaction starts with $\theta_H \cong 0$ and continues, the C^{s}_{HO} decreases with time due to slow H_2O_2 diffusion (the C^{s}_{HO}–t curve in Fig. 9(c)), and thus the H_2O_2-reduction current (j) decreases with time (the j–t curve). The decrease in j causes a decrease in the ohmic drop in the solution and hence a negative shift in E, which, in turn, leads to an increase in θ_H and leads to a further decrease in j. Here is also a positive feedback mechanism. Thus, when j reaches a certain critical value and θ_H enters into the region of rapid change with E (Fig. 6), the j suddenly decreases, accompanied by a sharp increase of θ_H from nearly zero to one (Fig. 9). The experimental results in Fig. 4 also show that sudden changes are triggered by critical values of j, as mentioned before.

It should be pointed out that this mathematical simulation is done by taking account of all plausible electrochemical reactions at the electrode surface, though in reported work[4,18–21] some main reactions are in general picked up to simplify the oscillation sytems for mathematical simulation. A rather complete treatment in this work has been made possible by the fact that the "H_2O_2–acid–Pt electrode" oscillation system has a stable Pt electrode and includes only

a small number of simple reactions. In this respect, this "H_2O_2–acid–Pt electrode" system may be regarded as a very suitable system for deep understanding of oscillation phenomena.

This work was partly supported by a Grant-in-Aid for Scientific Research on Priority Area, "Electrochemistry of Ordered Interfaces" No. 09237105 from the Ministry of Education, Science, Sports and Culture.

References

1) J. L. Hudson and T. T. Tsotsis, *Chem. Eng. Sci.*, **49**, 1493 (1994).
2) T. Z. Fahidy and Z. H. Gu, "Modern Aspects of Electrochemistry," ed by R. E. White, J. O'M. Bockris, and R. E. Conway, Plenum, New York (1995), Vol. 27, p. 383.
3) M. T. M. Koper, "Advances in Chemical Physics," ed by I. Prigogine and S. A. Rice, John Wiley & Sons, New York (1996), Vol. 92, p. 161.
4) U. F. Franck and R. FitzHugh, *Z. Elektrochem.*, **65**, 156 (1961).
5) S. Nakabayashi, K. Zama, and K. Uosaki, *J. Electrochem. Soc.*, **143**, 2258 (1996).
6) N. Shinohara, N. Kaneko, and H. Nezu, *Denki Kagaku*, **63**, 419 (1995).
7) K. Krischer, M. Luebke, W. Wolf, M. Eiswirth, and G. Ertl, *Electrochim. Acta*, **40**, 69 (1995).
8) S. Nakabayashi and A. Kira, *J. Phys. Chem.*, **96**, 1021 (1992).
9) H. Okamoto, N. Tanaka, and M. Naito, *Electrochim. Acta*, **39**, 2471 (1994).
10) H. Tributsch, *Ber. Bunsenges. Phys. Chem.*, **79**, 570 and 580 (1975).
11) H. Tributsch and J. C. Bennett, *Ber. Bunsenges. Phys. Chem.*, **80**, 321 (1976).
12) S. Cattarin and H. Tributsch, *J. Electrochem. Soc.*, **137**, 3475 (1990).
13) S. Cattarin, H. Tributsch, and U. Stimming, *J. Electrochem. Soc.*, **139**, 1320 (1992).
14) N. Fetner and J. L. Hudson, *J. Phys. Chem.*, **94**, 6506 (1990).
15) T. G. J. van. Verooij and M. T. M. Koper, *Electrochim. Acta*, **40**, 1689 (1995).
16) M. T. M. Koper, E. A. Meulenkemp, and D. Vanmaekelbergh, *J. Phys. Chem.*, **97**, 7337 (1993).
17) G. Flaetgen, K. Krisher, and G. Ertl, *J. Electroanal. Chem.*, **409**, 183 (1996).
18) M. T. M. Koper and J. H. Sluyters, *J. Electroanal. Chem.*, **303**, 73 (1991).
19) M. T. M. Koper and J. H. Sluyters, *J. Electroanal. Chem.*, **347**, 31 (1993).
20) L. Pohlmann, G. Neher, and H. Tributsch, *J. Phys. Chem.*, **98**, 11007 (1994).
21) M. T. M. Koper and D. M. Vanmaekelbergh, *J. Phys. Chem.*, **99**, 3687 (1995).
22) H. Hommura, Y. Mukouyama, T. Matsuda, S. Yae, and Y. Nakato, *Chem. Lett.*, **1996**, 391.
23) T. Matsuda, H. Hommura, Y. Mukouyama, S. Yae, and Y. Nakato, *J. Electrochem. Soc.*, **144**, 1988 (1997).
24) Y. Mukouyama, H. Hommura, T. Matsuda, S. Yae, and Y. Nakato, *Chem. Lett.*, **1996**, 463.
25) T. Matsuda, Y. Mukouyama, H. Hommura, S. Yae, and Y. Nakato, *J. Electrochem. Soc.*, **144**, 2997 (1997).
26) R. Gerischer and H. Gerischer, *Z. Phys. Chem. N. F.*, **6**, 178 (1956).
27) V. D. Winkelmann, *Z. Elektrochem.*, **60**, 731 (1956).
28) R. Memming, *J. Electrochem. Soc.*, **116**, 785 (1969).
29) A. J. Bard and L. R. Faulkner, "Electrochemical Methods, Fundamentals and Applications," John Wiley & Sons, New York (1980), p. 540.
30) R. J. Nichols and A. Bewick, *J. Electroanal. Chem.*, **243**, 445 (1988).
31) H. Kita, Y. Gao, S. Ye, and K. Shimazu, *Bull. Chem. Soc. Jpn.*, **66**, 2877 (1993).
32) N. Tanaka and R. Tamamushi, *Electrochim. Acta*, **9**, 963 (1964).
33) D. M. H. Kern, *J. Am. Chem. Soc.*, **76**, 4208 (1954).
34) J. J. Lingane and P. J. Lingane, *J. Electroanal. Chem.*, **5**, 411 (1963).
35) V. G. Prabhu, L. R. Zarapkar, and R. G. Dhaneshwar, *Electrochim. Acta*, **26**, 725 (1981).
36) P. W. Atkins, "Physical Chemistry," 4th ed, Oxford University Press, Oxford (1990).